Applied Catalysis B: Environmental 95 (2010) 130–136

Contents lists available at ScienceDirect

Applied Catalysis B: Environmental

journal homepage: www.elsevier.com/locate/apcatb

TiO_2–MCM-41 for the photocatalytic abatement of NOx in gas phase

M. Signoretto [a,*], E. Ghedini [a], V. Trevisan [a], C.L. Bianchi [b], M. Ongaro [b], G. Cruciani [c]

[a] Dipartimento di Chimica, Università Cà Foscari, Consortium INSTM-RU of Venice, Calle Larga Santa Marta, 2137, 30123 Venice, Italy
[b] Dipartimento di Chimica Fisica ed Elettrochimica, università degli Studi di Milano, Consorzio INSTM_RU Milano, Via Golgi 19, 20133 Milan, Italy
[c] Dipartimento di Scienze della Terra, Università diFerrara, Via Saragat 1, I-44100 Ferrara, Italy

ARTICLE INFO

Article history:
Received 4 November 2009
Received in revised form 9 December 2009
Accepted 17 December 2009
Available online 24 December 2009

Keywords:
Nanotitania
Mesoporous silica
NOx oxidation
Photocatalysis

ABSTRACT

Nanotitania supported on mesoporous silica systems were synthesized by a reliable procedure based on an incipient wetness impregnation post-synthetic approach. Characterization by X-ray diffraction, N_2 physisorption, TEM, X-ray photoelectron spectroscopy, ICP has been carried out in order to investigate the chemical–physical properties of the catalysts with particular attention to the chemical nature of the titanium species. The photocatalytic activity of the samples was evaluated for the degradation of NOx in the gas phase. The influence of both the textural properties and the nature of titanium species on the photocatalytic activity is discussed.

1. Introduction

Titanium dioxide is one of the most common materials in everyday life. It has been widely used as white pigment in paints, cosmetics and foodstuffs and in recent years photocatalytic processes using TiO_2 have been applied to important problems of environmental interest like purification of water and air. TiO_2 is a semiconductor with a band gap energy E_g = 3.2 eV (this value is that of the anatase form); when this material is irradiated with photons (e.g. sunlight) the electron–hole pair that is created may separate and the resulting charge carriers might migrate to the surface where they can react with adsorbed water and oxygen to produce radical species. These attack any adsorbed organic molecule and can lead to complete decomposition into CO_2 and H_2O [1]. Compared with traditional advanced oxidation processes the technology of photocatalysis is known to have some advantages, such as ease of setup and operation at room temperatures, no need for post-processes, low consumption of energy and consequently low costs, high degradation efficiency in removing organic pollutants even at ultra low concentrations. For the realization of these practical applications, development of highly active photocatalysts is keenly desired. Based on the kinetic investigation of photocatalytic reactions, TiO_2 nanoparticles in the anatase crystal form having both high crystallinity and large surface area [2] must exhibit higher photocatalytic activity. This last property should increase the amount of surface-adsorbed substrate to enhance the capture of photogenerated electron and positive hole. The control of the final features of the oxide can be achieved by several approach among that: sol–gel synthesis [3], by employing surfactants [4,5] and more recently there has been increasing interest in introducing titanium into high surface area support materials. Good candidates for supports are mesostructured silicas because of their high surface areas, ordered frameworks, and narrow pore size distribution [6–9].

Several approaches can be adopted for the synthesis of high area mesoporous silica/titania systems that can be divided in two classes:

(i) introduction of TiO_2 during the formation of the silica material (one-pot synthesis) [10–12].
(ii) introduction of TiO_2 in a pre-synthesized silica support by applying post-synthesis methods: acid-catalysed sol–gel method, chemical solution deposition, multistep deposition [9–15].

The first approach permits an accurate control of the final properties of the titania/silica catalyst by varying the variables involved in the synthesis process but at the same time requests a careful control of the reactivity of the Ti- and Si-precursors that have to be adjusted to each other. This is the most critical step (very hard in some cases) of the synthesis process and the successfully realization of the final composite (TiO_2/SiO_2) is strictly dependent to it. Post-modification is a more practical pathway for to obtain silica/titania catalysts but often does not permit an accurate control on the incorporation of the TiO_2 particles at the different

* Corresponding author. Tel.: +39 041 2348650; fax: +39 041 2348517.
E-mail address: miky@unive.it (M. Signoretto).

0926-3373/$ – see front matter © 2009 Elsevier B.V. All rights reserved.
doi:10.1016/j.apcatb.2009.12.019

location within the porous structure, namely inside or outside of the mesoporous channel, whereby a possible blocking of the pore apertures can occur. Obtaining the required full information about the actual position of TiO_2 nanoparticles is usually a very difficult task [9]. In any case, the review of literature works suggests that an ideal and general approach for the synthesis of supported nanotitania does not exist. On the contrary, *ad hoc* preparation methods must be chosen in order to account for the specific requirements of final applications.

The twofold goal of this work is to establish first a new preparation method to produce titania/silica catalysts characterized by high surface area and ordered pore structure for photocatalytic applications. Such an aim can be accomplished by supporting the TiO_2 particles on MCM-41 mesoporous silica via an incipient wetness impregnation using $Ti(iOPr)_4$ as a precursor. Particular attention has to be paid to the influence of the TiO_2 amount on the chemical–physical properties of the final systems. In fact, different Ti loadings in the catalysts may induce changes not only in the textural characteristics but also in the surface chemical properties of the TiO_2/SiO_2 composites. As a second goal, the catalytic behaviour of the investigated systems will be tested towards the photocatalytic abatement of NOx in gas phase. This part of the study will be focussed, in particular, on the preliminary assessment of the critical parameter involved in the catalytic process.

2. Experimental

2.1. Synthesis

The MCM-41 support was prepared as reported in a previous work [16]. The surfactant was removed from the as-synthesized MCM-41 silica by calcination in air at 540 °C for 6 h.

The silica support was activated with TiO_2 by incipient wetness impregnation by using an alcoholic solution of $Ti(iOPr)_4$. The obtained Ti/MCM-41 composites were dried at 80 °C for 12 h and finally calcined at 500 °C in flowing air (30 mL/min) for 3 h. Five samples with increasing Ti/Si ratio (9 wt%, 17 wt%, 23 wt%, 28 wt%, 33 wt%) have been prepared. The calcined samples are labelled 'TM*x*' where 'T' stands for TiO_2, 'M' for MCM-41 and *x* for the TiO_2 effective content of catalyst.

2.2. Sample characterization

Specific surface area and pore size distribution were obtained from N_2 adsorption–desorption isotherms at 77 K (MICROMERITICS ASAP 2000 Analyser). Surface area was calculated by the BET equation [17], whereas the mesopore size distribution was determined by the BJH method [18], applied to the N_2 adsorption isotherm branch.

X-ray diffraction (XRD) patterns of the samples were collected by a Bruker D8 Advance powder diffractometer equipped with a sealed X-ray tube (copper anode; operating conditions, 40 kV and 40 mA) and a Si(Li) solid state detector (Sol-X) set to discriminate the Cu Kα radiation.

X-ray photoelectron spectra were taken in a M-probe apparatus (Surface Science Instruments). The source was monochromatic Al K_α radiation (1486.6 eV). A spot size of 200 μm × 750 μm and pass energy of 25 eV were used. The energy scale was calibrated with reference to the $4f_{7/2}$ level of a freshly evaporated gold sample, at 84.00 ± 0.1 eV, and with reference to the $2p_{3/2}$ and 3s levels of a copper at 932.47 ± 0.1 and 122.39 ± 0.15 eV, respectively. The binding energies (BE) were corrected for specimen charging by referencing the C 1s peak to 284.6 eV, and the background was subtracted using the Shirley's method. The C region was fitted into two or three peaks, depending on the tail shape. The fitting was performed using only Gaussian line shapes without BE or full width at half maximum (FWHM) constraints.

Transmission electron microscopy (TEM) images were taken using a JEOL JEM 2000EX. Aliquots of each powder sample were suspended in isopropyl alcohol, sonicated for 5–10 min so that the particles were well dispersed and deposited on a holey carbon film.

The Ti content in the final solid products was determined by inductively coupled plasma emission spectroscopy (ICP).

2.3. Catalytic test

The photocatalytic activity of samples has been evaluated in the NOx oxidation reaction and the experimental apparatus was schematized in Fig. 1. The gas phase reaction was carried out in a fixed-bed reactor at atmospheric pressure and room temperature by feeding 2780 mL/min of the reaction mixture (NO/air, 100 ppb of NO). In a typical experiment the catalysts (50 mg), previously ground and sieved to 50–70 mesh (0.2–0.3 mm), were introduced into a 2 mm internal diameter microreactor irradiated with an UV lamp (mercury vapour lamp, spectral range 315–400 nm, power 125 W; Helios Italquartz, GN125RZS). The measured irradiance on the sample was 8.50 W/m^2.

NO and NO_2 were monitored in continuous with an AC32M chemiluminescent oxide nitrogen analyser.

The catalytic efficiency is measured as conversion of NO, calculated with the following equation:

$$\text{conversion} = \frac{C_i - C_m}{C_i} \times 100 \quad (1)$$

where C_i is the initial concentration of NO and C_m is the minimal concentration of NO.

3. Results and discussion

3.1. Optimization of working conditions

A preliminary study was carried out in order to determine the optimal working conditions for the catalytic test. In particular, the

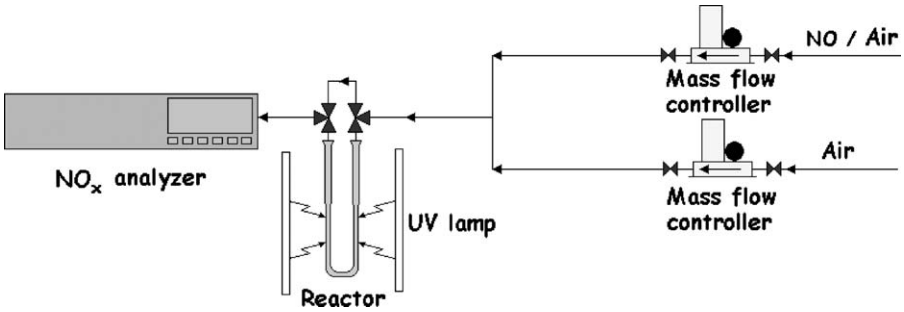

Fig. 1. Experimental apparatus for NO oxidation.

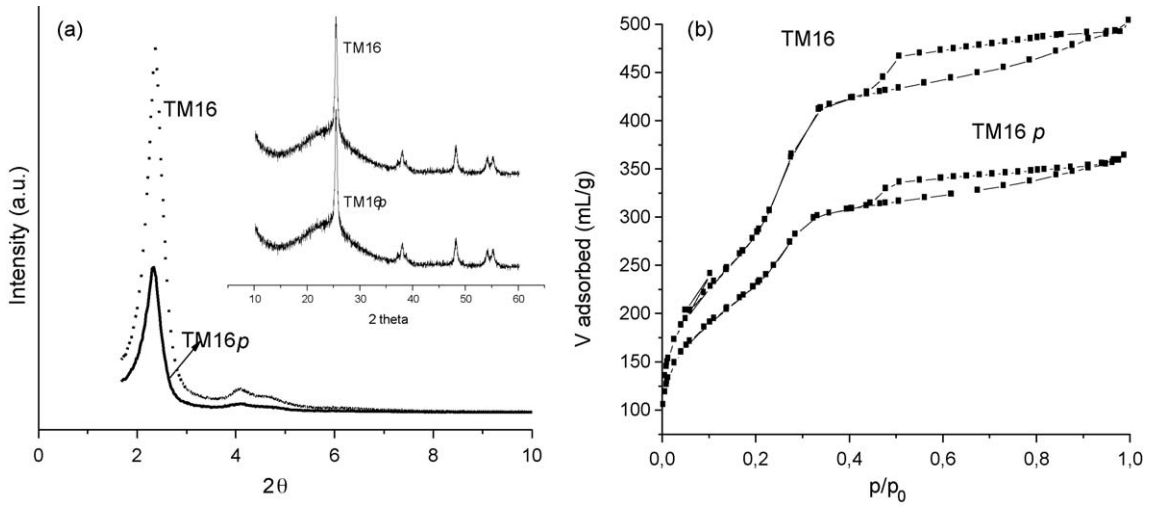

Fig. 2. (a) Diffraction patterns of TM16 sample before and after mechanical pressing; (b) adsorption–desorption isotherms of TM16 sample before and after mechanical pressing. Sample after pressing is labelled 'TM16p'.

high activity of the catalysts required the minimization of the contact time between the catalytic bed and the reagent species. This condition is necessary to allow an effective evaluation of the performance of the investigated samples. This aim was pursued by choosing the best compromise between the power of irradiation, the amount of catalyst and the feed mixture rate. In particular it was found necessary to use an elevated gas flow which, as a drawback, can lead to an increased packing of the catalytic bed. To avoid this problem the samples were pressed, ground and sieved, before submitting them to the catalytic test. The influence of the moulding process on the crystal structure of catalysts was evaluated by XRD. Powder diffraction patterns of the TM16 sample are reported in Fig. 2; similar results were obtained for all the other samples (not reported here).

As far as the mesoporous support is concerned, Fig. 2 shows that the MCM-41 typical peaks in the low angle region of the XRD pattern do not disappear after pressing the sample, but only exhibit a slight decrease in intensity. This suggests that the ordered structure of MCM-41 is substantially retained. Concerning the TiO_2 anatase phase, the comparison of XRD patterns in the high angle region shows that the crystalline active phase is totally unaffected by the preliminary mechanical treatment.

Physisorption analyses show a slight decrease of surface area and pore volume in all the pressed samples (Table 1) suggesting that pressure causes blocking of some pores while leaving the shape of the isotherm almost unchanged (see Fig. 2(b) for the TM16 system). It is worth noting that the surface area values (see Table 1) of all the pressed catalysts are high (>600 m^2/g). All these results confirm that the moulding process does not substantially alter the textural properties of the catalysts and permits the retention of the structural and morphological features (in particular high surface area and TiO_2 crystallinity) that are the first and indispensable requirements of the prepared materials.

3.2. Catalytic test

After optimization of the critical parameters involved in the catalytic test, the photo-activity of the SiO_2/TiO_2 systems was evaluated in the NOx oxidation reaction as described in Section 2. The NO and NO_2 concentrations were monitored in continuous and a profile of such concentrations as a function time was recorded (see Fig. 3 for a representative plot). As shown the NO concentration reaches a minimum value followed by a slow and continuous deactivation process after the adsorption of NO_3^- on the catalytic active sites.

Based on the above considerations, the minimum value of the concentration of NO was employed as parameter for the evaluation of the catalytic performances. The catalytic efficiency was measured as the NO conversion, calculated by Eq. (1).

The catalytic results obtained for all the samples are represented in Fig. 4. As expected, the pure silica MCM-41 support was catalytically inactive in the reaction while all the TiO_2/MCM-41 catalysts were active in our experimental work conditions, and showed good conversion values.

Surprisingly, the conversion values were found to be not proportionally related with the amount of the active phase. In fact,

Table 1
Chemical–physical data of MCM-41 support and of all TiO_2/SiO_2.

Sample	%wt TiO_2 effective	BET surface area (m^2/g)	Pore diameter (nm)	Total pore volume (mL/g)
MCM-41	0	1344	2.8; 4	0.86
TM9	9	1076	2.8; 4	0.92
TM16	16	989	2.3; 3.8	0.72
TM22	22	881	2.3; 3.7	0.72
TM28	28	799	2.5; 4	0.73
TM32	32	803	2.5; 3.9	0.57
TM9p	9	851	3.2	0.68
TM16p	16	836	3.0	0.60
TM22p	22	805	2.3; 3.6	0.60
TM28p	28	700	2.5; 4	0.50
TM32p	32	698	2.4; 3.5	0.48
p25	100	52	11	0.13

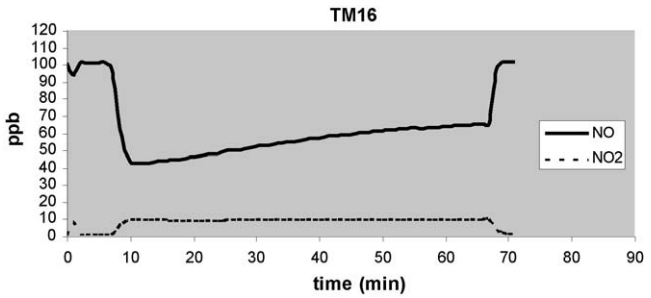

Fig. 3. Concentration profile of NOx for the photo-oxidation of NO.

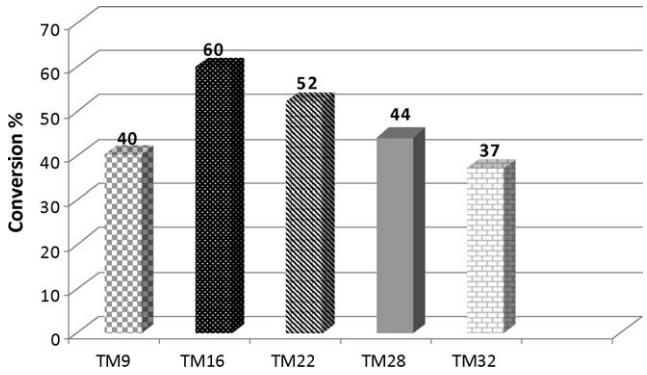

Fig. 4. Catalytic results for the NO oxidation reaction.

the best performance was reached by the TM16 catalysts containing a 16 wt% TiO_2 content. The increase of TiO_2 loading over the former value did not improve the catalytic activity; on the contrary a progressive decrease of the conversion rates was observed as the TiO_2 concentration increased from 16 to 32 wt% (see Fig. 4). The catalytic performance of our systems was compared with that of a commercial TiO_2; we have used as reference frames a 100% P25 catalyst and a P25 oxide (16 wt%) supported on the MCM-41 silica matrix. The conversion value achieved from the 100% TiO_2 catalyst was comparable (58%) to that obtained from the best TiO_2/MCM-41 system (60%); on the contrary, the maximum NO conversion reached from the P25/MCM-41 composite was the 35% that, at the same content of active phase, is decidedly worse than that exhibited from the systems investigated in the present work. This result reveals that could exist a real advantage from the application of the TiO_2/MCM-41 in the photocatalytic NOx abatement.

3.3. Chemical–physical characterization

In order to clarify the unexpected behaviour of the catalytic activity vs. the TiO_2 content, the effects of several variables were analyzed and discussed. The considered variables are those related to the chemical–physical properties as determined and listed in Table 1 for the studied materials.

The effective amount of TiO_2 (see Table 1) was evaluated by ICP analyses. All the catalysts were prepared twice in order to check for reproducibility: in all the cases the double measured values were found to be within the error range. These results provide strong evidence for a large reliability of the method we used for the preparation of catalysts.

The textural properties were evaluated by N_2 physisorption analyses and the measured pore size distributions are reported in Fig. 5. For pure MCM-41 the physisorption measurements follow the type IV isotherm, with hysteresis between the adsorption and the desorption branches, in agreement with the literature data for silica materials treated at 540 °C [19], the same calcination temperature as our samples. Moreover, the isotherms of all TiO_2/MCM-41 show the typical profile of a mesoporous material although some differences appear when compared to those of the pure silica support.

The volume of the adsorbed gas decreases with the increase of the load of the active phase accompanied by a diminution of the BET surface area (see Table 1). The pore size distribution is bi-modal for all the modified systems characterized by a second peak corresponding to a pore diameter centred at about 4 nm. This last feature can be plausibly related to a partial collapse of the porous

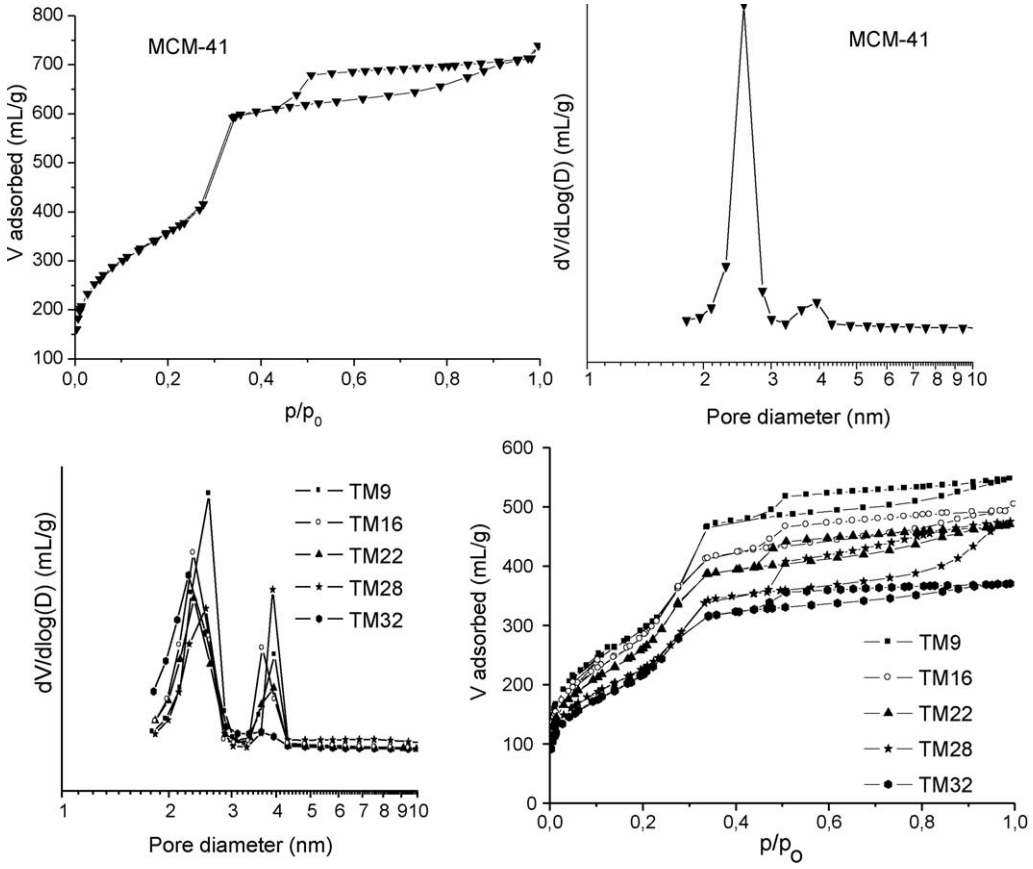

Fig. 5. Adsorption–desorption isotherms and pore size distributions for MCM-41 and for all the TiO_2/SiO_2 catalysts.

structure after the introduction of the active phase, in particular as consequence of the second calcination treatment. On the other hand, the existence in all the catalysts of a substantial fraction of pores at about 2.5 nm, thus smaller than those in the silica support (2.8 nm) suggests, together with the decrease of total pore volume (see Table 1), the presence of a fraction of TiO_2 within the channels of MCM-41.

Despite the variations of both surface area and pore size, the shape of the isotherm is retained after the introduction of TiO_2 nanoparticles, indicating that the mesoporous morphology of the support has been preserved. On the other hand, the mesoporous texture of the systems could have been more heavily compromised by higher TiO_2 loadings. This suggests that an excessive amount of the active phase could be detrimental to the catalytic efficiency which also relies on the transport of reacting species through the open channel system. The diminution of surface area with the increase of the TiO_2 content could be, in fact, one of the possible causes for the lower catalytic activity exhibited by the sample with TiO_2 load higher than 16 wt%.

It is well known that, in addition to the surface area, the type of crystalline phase of TiO_2 also affects the catalytic performances. In order to obtain information about the crystal structure properties of the TiO_2 nanoparticles, X-ray diffraction (XRD) and transmission electron microscopy (TEM) analyses have been carried out.

The diffraction patterns at low 2θ angles for the pure silica support and for all TiO_2/MCM-41 samples are reported in Fig. 6. The XRD pattern of MCM-41 (inset Fig. 6) shows the presence of the characteristic low angle reflections due to the periodically ordered structure characteristic of a hexagonal symmetry (*p6mm*); there are some significant differences between the diffraction profiles of catalysts and that of the parent support. For all titania/silica samples, the presence of a well resolved peak, corresponding to the reflection of the (1 0 0) plane, whose intensity decreases and the broadening increases with the amount of TiO_2 is evident. This observation can be interpreted as due to a degradation of the periodic mesostructure of silica supports which might have occurred upon the incorporation of the active phase. Alternatively, it has been suggested by Sauer et al. [20] that a reduction of the peak intensity does not necessarily reflects a pore collapse but could also be explained by the incoherent character of X-rays scattered by a disordered distribution of TiO_2 nanoparticles inserted within the mesoporous channels.

So it can be speculated that even if the lattice parameter were affected by the presence of TiO_2, the ordered structure of all the silica supports has been retained to a certain degree in all the catalysts, in agreement with the physisorption results.

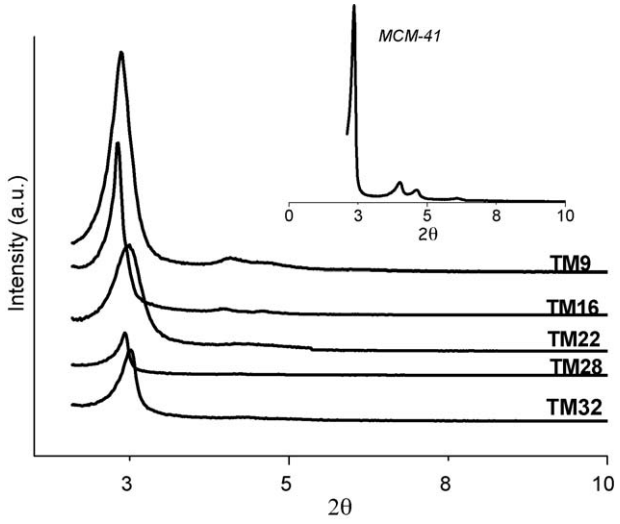

Fig. 6. X-ray powder diffraction patterns in the low 2θ region of MCM-41 (inset figure) and of catalysts.

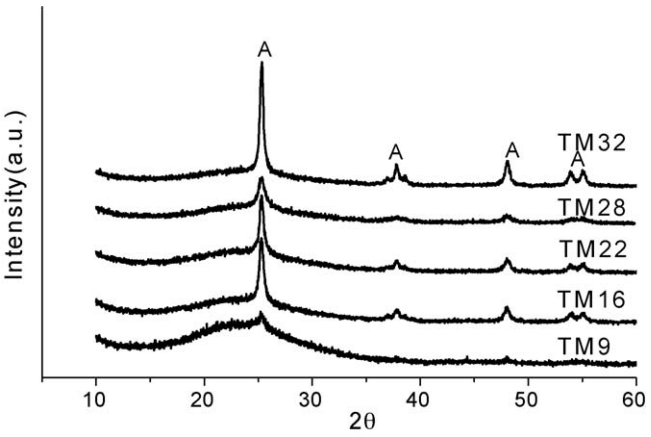

Fig. 7. X-ray powder diffraction patterns in the 2θ region of TiO_2 phases (A: anatase phase).

The high 2θ angle region of XRD patterns of all TiO_2/MCM-41 samples, as reported in Fig. 7, shows that anatase is the only TiO_2 phase found in all samples. In Fig. 8 the integrated intensities of the main anatase peak at $2\theta = 25.3^\circ$ and the broad hump centred at about 24.4° 2θ are plotted as a function of TiO_2 content. The anatase peak intensity scales positively with the TiO_2 content although with a non-perfectly linear trend. The inverse relationship with the broad hump intensity is expected on the basis of the relative variations of phase fractions in the (pseudo-)binary mixture and the contrast in mass X-ray absorption coefficients of TiO_2 and SiO_2 phases. The above trends suggest that the X-ray amorphous phase (most likely SiO_2-rich) decreases with the increasing crystalline anatase content. However, it cannot be ruled out that a TiO_2 poorly crystalline phase might contribute to the integrated intensity of the hump.

The crystal size of anatase was also estimated from a Double-Voigt analysis [21] of the XRD peak broadening performed by a Rietveld fit using the Bruker Topas program [22]. The anatase crystal size was found to vary from 7(2) nm in TM9, to 11(1) nm in TM16, to 8(1) nm in TM22, to 7(2) nm in TM28, and to 15(1) nm in TM32.

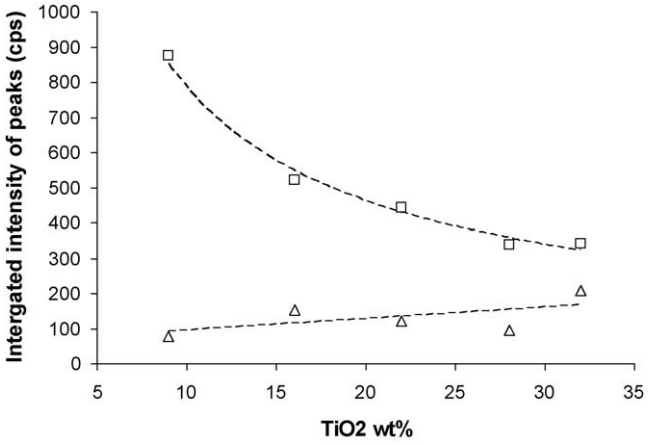

Fig. 8. Integrated XRD intensity for the main anatase peak at $2\theta = 25.3^\circ$ (triangles) and the broad hump centred at about 24.4° 2θ (squares) as a function of TiO_2 content of catalysts.

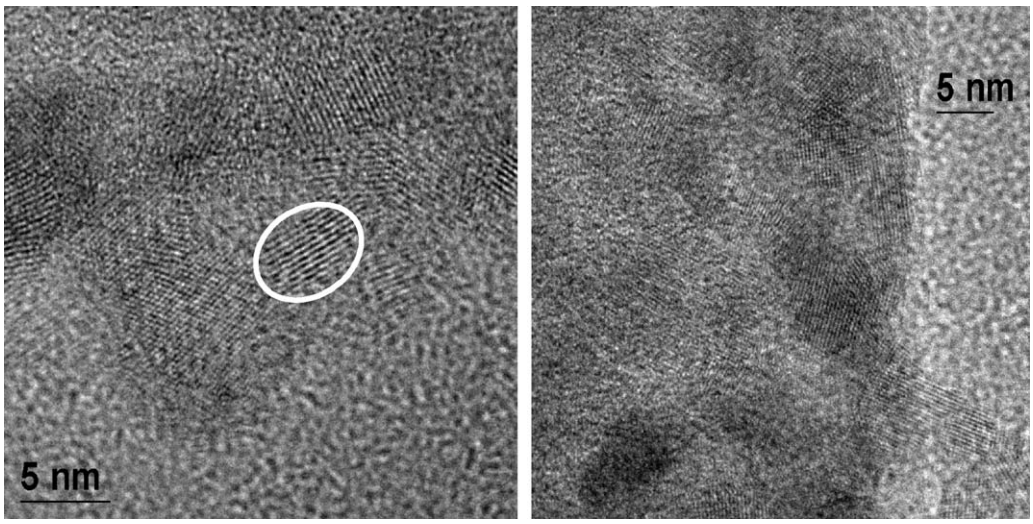

Fig. 9. HR-TEM images of TM16 and TM28 samples.

In order to obtain further information about the size of anatase nanocrystals and explore their relationships with respect to the mesoporous support, high-resolution TEM images were collected. The micrographs obtained for the TM16 and TM28 samples are reported in Fig. 9; very similar images were observed for the other samples (not reported here). As we can observe the overgrowth of titania on the external surface of the pore channels of the silica support is evident. The dimensions of TiO_2 nanoparticles are centred about 7 nm for both samples in a reasonable agreement with the XRD analysis. As also observed by XRD, anatase is the only TiO_2 phase detected.

The structural data characterizations can be summed up briefly with the following considerations:

(i) the introduction of TiO_2 on the silica support affected partially the structural integrity of the MCM-41 but the mesoporous order is retained to a certain degree in all the catalysts;
(ii) only nanocrystalline TiO_2 in the anatase phase was detected in all the systems;
(iii) the X-ray amorphous phase detected in all the composites decreases with the increasing crystalline anatase content.

In the light of the reported data we can conclude that the textural features of the catalysts, although some differences have been detected, are not enough marked to explain the catalytic results. TM16 and TM22 samples are characterized by the best compromise between surface area, ordered structure and crystalline anatase content that justify partly their high catalytic activity; however, this is not sufficient to interpret the catalytic trend in particular the progressive decrease of the conversion rates observed as the TiO_2 concentration increased from 22 to 32 wt%. In order to gain more information about the surface chemical properties of the systems and to investigate thoroughly their catalytic behaviour XPS was resorted on.

Survey XPS spectra were recorded for all samples. No signicant presence of impurities was observed, except for the ubiquitous presence of carbon contaminant.

The Ti/Si atomic ratios of the present samples are reported in Table 2 (2nd column). As expected the values monotonically increase by increasing the Ti content in the samples.

The features of peak corresponding to the Ti 2p binding energy (BE) are not regular along the series of measured samples. Only in TM22 it was the Ti $2p_{3/2}$ peak occurring at a binding energy of 458.6 ± 0.2 eV which is typical of Ti(IV) in the oxide [3,23]. The rest of samples showed a doublet suggesting the occurrence of different Ti species ($Ti^{(4-delta)+}$ and $Ti^{(4+delta)+}$). More in detail (Fig. 10), samples with lower Ti content showed the presence of a shoulder at lower BE (457.0 ± 0.2 eV) (with a $Ti^{(4-delta)+}$ content of 30% and 6% for TM9 and TM16, respectively) up to its complete disappearance in TM22 sample. A further increase of Ti amount led to the formation of a new species at higher BE (459.9 eV). In this case the $Ti^{(4+delta)+}/Ti^{+4}$ ratio increases by increasing the amount of Ti content (from 13% to 78% for TM 28 and TM32, respectively). Both the species $Ti^{(4+delta)+}$ and $Ti^{(4-delta)+}$ are of uncertain attribution but they can be plausibly associated with the interaction between the Ti species and the support. When the titanium concentration is low the Ti–silica interaction is strong and the TiO_2 electrons are attracted from the support that explain the existence of the $Ti^{(4-delta)+}$ species, the opposite effect can explain the presence of the $Ti^{(4+delta)+}$ species for higher amount of Ti [24].

XPS results are in good agreement with the catalytic performance of the samples being TM16 the most efficient photocatalyst followed by TM22. It is well known that the pure anatase form (TM22, one XPS species at 458.8 eV) is the most active in a photocatalytic reaction, but the presence of a small amount of substoichiometric TiO_2 (TM16) could slow down the electron–hole recombination, close of the photocatalytic processes, and improve the sample efficiency. In all other cases, the presence of a larger and larger content of the $Ti^{(4+delta)+}$ species brings about a progressive efficiency loss of the photocatalyst.

Table 2
Ti/Si atomic ratio and binding energy (Ti 2p) of all the catalysts obtained from XPS data fitting.

Sample	Ti/Si atomic ratio	B.E. $2p_{3/2}$ (eV)
TM9	0.2	457.2 (30%) 458.6 (70%)
TM16	0.5	456.9 (6%) 458.5 (94%)
TM22	1.7	458.6 (100%)
TM28	2.3	458.5 (87%) 459.9 (13%)
TM32	2.7	458.5 (22%) 459.9 (78%)

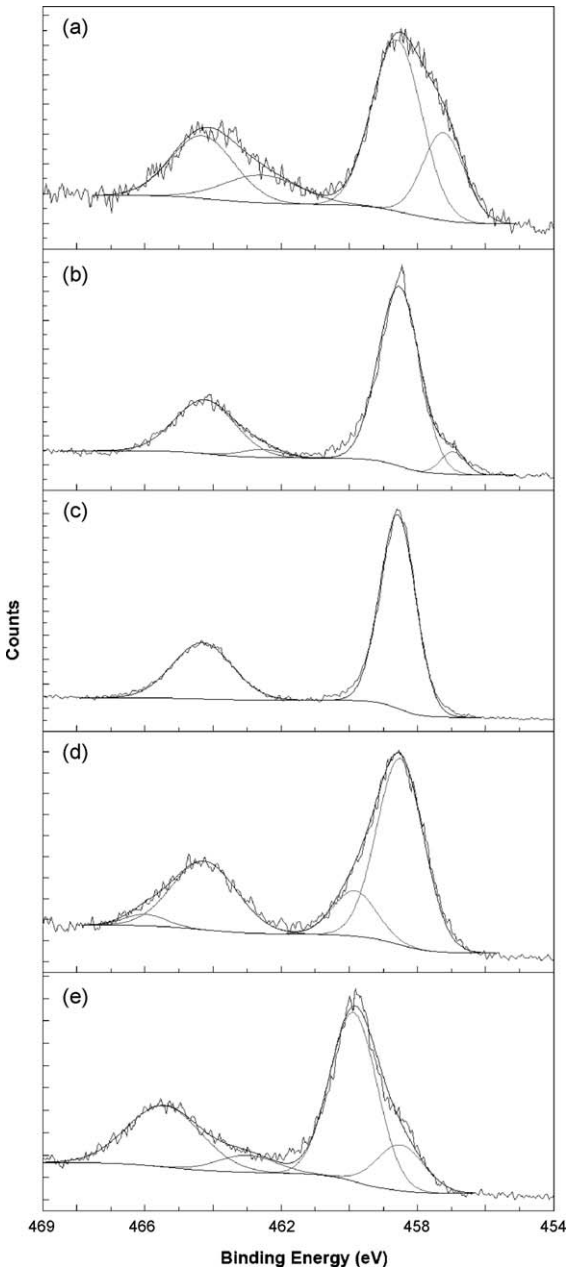

Fig. 10. Ti 2p XPS spectra: (a) TM9, (b) TM16, (c) TM22, (d) TM28, (e) TM32.

4. Conclusions

This work demonstrated that the incorporation of titanium on MCM-41 by incipient wetness impregnation is a reliable method for the synthesis of silica-supported titania nanoparticles (size down to about 7 nm) with the retention of the mesoporous structure of the support (ordered structure and high surface area). The NOx oxidation, employed as test reaction, was strongly influenced by the degree of TiO_2 loading and good performances could be achieved by an optimal compromise between surface area, crystalline form and the chemical environmental around the active site. The best catalytic behaviour was found for the sample with a TiO_2 content of 16 wt% showing an high percentage of TiO_2 in the anatase form accompanied with a small amount of sub-stoichiometric TiO_2 that likely helped to improve the catalytic sample efficiency. The obtained results showed that the application of these catalysts is well suitable in gas photocatalytic reactions (inorganic pollutants degradation). In particular, the surface area and pore size dimensions are expected to play a central role which can be modulated by the opportune choice of the mesoporous support as showed in our work.

Acknowledgement

The authors want to thank Mrs. Tania Fantinel for the excellent technical assistance.

References

[1] A. Mills, H.R. Davies, D. Worsley, Chem. Soc. Rev. 22 (1993) 417–425.
[2] S. Bakardjieva, V. Stengl, L. Szatmary, J. Subrt, J. Lukac, N. Murafa, D. Niznansky, K. Cizek, J. Jirkovskyc, N. Petrova, Mater. Chem. 16 (2006) 1709–1716.
[3] S. Ardizzone, C.L. Bianchi, G. Cappelletti, S. Gialanella, C. Pirola, V. Ragaini, J. Phys. Chem. C 111 (2007) 13222–13231.
[4] G. Cappelletti, C.L. Bianchi, S. Ardizzone, Appl. Surf. Sci. 253 (2006) 519–524.
[5] P. Yang, D. Zhao, D.I. Margolese, B.F. Chmelka, G.D. Stucky, Nature 396 (1998) 152–155.
[6] N.B. Lihitkar, M.K. Abyaneh, V. Samuel, R. Pasricha, S.W. Gosavi, S.K. Kulkarni, J. Colloid Interface Sci. 314 (2007) 310–316.
[7] E. Beyers, E. Biermans, S. Ribbens, K. De Witte, M. Mertens, V. Meynen, S. Bals, G. Van Tendeloo, E.F. Vansant, P. Cool, Appl. Catal. B: Environ. 88 (2009) 515–524.
[8] K. De Witte, A.M. Busuioc, V. Meynen, M. Mertens, N. Bilba, G. Van Tendeloo, P. Cool, E.F. Vansant, Micropor. Mesopor. Mater. 110 (2008) 100–110.
[9] R. Van Grieken, J. Aguado, M.J. López-Muños, J. Marugán, J. Photochem. Photobiol. A 148 (2002) 315–322.
[10] Y. Chen, Y. Huang, J. Xiu, X. Han, X. Bao, Appl. Catal. A: Gen. 273 (2004) 185–191.
[11] X. Zhang, F. Zhang, K.-Y. Chan, Appl. Catal. A: Gen. 284 (2005) 193–198.
[12] Y. Li, S.-J. Kim, J. Phys. Chem. B 109 (2005) 12309–12315.
[13] S. Perathoner, P. Lazafame, R. Passalacqua, G. Centi, R. Schlögl, D.S. Su, Micropor. Mesopor. Mater. 90 (2006) 347–361.
[14] W. Wang, M. Song, Micropor. Mesopor. Mater. 96 (2006) 255–261.
[15] H. Ding, H. Sun, Y. Shan, J. Photochem. Photobiol. A 169 (2005) 101–107.
[16] E. Ghedini, M. Signoretto, F. Pinna, G. Cerrato, C. Morterra, Appl. Catal. B: Environ. 67 (2006) 324–336.
[17] S. Brunauer, P.H. Emmett, E. Teller, J. Am. Chem. Soc. 60 (1938) 309–319.
[18] E.P. Barrett, L.G. Joyner, P.P. Halenda, J. Am. Chem. Soc. 73 (1951) 373–380.
[19] B. Muñoz, A. Rámila, J. Pérez-Pariente, I. Díaz, M. Vallet-Regi, Chem. Mater. 15 (2003) 500–503.
[20] J. Sauer, F. Marlow, F. Schüt, Phys. Chem. Chem. Phys. 3 (2001) 5579–5584.
[21] D. Balzar, in: R.L. Snyder, H.J. Bunge, J. Fiala (Eds.), Voigt-function Model in Diffraction Line-broadening Analysis—Microstructure Analysis from Diffraction, International Union of Crystallography, 1999.
[22] Bruker AXS, TOPAS V4: General Profile and Structure Analysis Software for Powder Diffraction Data—User's Manual, Bruker AXS, Karlsruhe, Germany, 2008
[23] J.F. Moulder, W.F. Stickle, K.D. Bomben, Handbook of X-ray Photoelectron Spectroscopy, PerkinElmer, Eden Praie, 1992.
[24] R.P. Netterfield, P.J. Martin, C.G. Pacey, W.G. Sainty, J. Appl. Phys. 66 (4) (1989) 1805.